Collective entanglement in quantum materials with competing orders

Giacomo Mazza and Costantino Budroni
Department of Physics "E. Fermi" University of Pisa, Largo B. Pontecorvo 3, 56127 Pisa, Italy

We investigate entanglement detection in quantum materials through criteria based on the simultaneous suppression of collective matter excitations. Unlike other detection schemes, these criteria can be applied to continuous and unbounded variables. By considering a system of interacting dipoles on a lattice, we show the detection of collective entanglement arising from two different physical mechanisms, namely, the ferroelectric ordering and the dressing of matter degrees of freedom by light. In the latter case, the detection shows the formation of a collective entangled phase not directly related to spontaneous symmetry breaking. These results open a new perspective for the entanglement characterization of competing orders in quantum materials, and have direct application to quantum paraelectrics with large polariton splittings.

Introduction.— Entanglement plays a pivotal role in characterizing collective behavior in quantum matter. Collective entanglement is naturally linked to the presence of quantum critical behaviour associated with spontaneous symmetry breaking [1–4]. However, entanglement can also become a distinctive feature of systems in which quantum collective behavior remains elusive due to the absence of explicit symmetry breaking. This is evident in cases such as spin liquids, Mott insulators, or other types of topological orders [5–8]. This becomes even more relevant in quantum materials characterized by multiple orders emerging from competing collective behaviors [9, 10].

Entanglement detection is now achievable across various quantum systems and degrees of freedom, employing a wide array of methods [11–13]. These methods range from the exact reconstruction of the density matrix for few-particle systems to entanglement witnesses based solely on measuring a limited number of collective variables. The latter approach is particularly pertinent for many-body systems, especially materials, which often lack the level of tunability found in simpler systems. In recent years, the quantum Fisher information (QFI) [14, 15] associated with a collective variable has emerged as a powerful technique for detecting entanglement [16–18]. This is particularly evident in quantum materials, where it has been linked to the measurement of dynamical susceptibilities achievable through state-of-the-art spectroscopic techniques [3, 19–24]. The QFI establishes a connection between entanglement and large collective quantum fluctuations, serving as an entanglement witness when it surpasses a certain threshold, namely its maximum value across all separable states. However, its applicability is confined to collective excitations with bounded spectra, such as spin degrees of freedom. Yet, collective excitations within quantum materials typically encompass observables with unbounded spectra, such as position and momentum. Consequently, the practical implementation of QFI detection schemes is constrained by the determination of the bound itself [25, 26]. A way around this problem is suggested by the observation that entanglement is also revealed by small quantum fluctuations. Famous examples include spin-squeezing phenomena [27–30] as well as the Einstein-Podolsky-Rosen (EPR) argument [31] with the associated vanishing uncertainties for the center of mass position and relative momentum [32, 33].

Here, we apply criteria based on the simultaneous suppression of collective excitations to the detection of entanglement emerging from competing orders in quantum matter. We consider a quantum paraelectric as a prototype system in which collective behavior can emerge from the interplay between ferroelectric quantum criticality [34–37], and the collective dressing by strong light-matter coupling at equilibrium [38–44]. Entanglement is witnessed by the simultaneous suppression of the collective excitations which anti-correlate, respectively, with the incipient ferroelectric ordering and the formation of polaritons. These two different types of detection schemes are intuitively related to two different physical mechanisms of formation of entanglement. In the former case, entanglement is a direct consequence of intrinsic quantum critical behavior. In the latter case, entanglement is transferred, in thermal equilibrium, from photons to matter degrees of freedom. We show that the witness associated with ferroelectricity is made entanglement-blind by the light-matter interaction and vice versa, thus highlighting the competing nature of the two origins of collective entanglement. The detection scheme is completely general and can be applied to any system whose relevant excitations are described by pairs of conjugate variables.

Model and entanglement criteria.— We consider a system of N one-dimensional quantum oscillators of mass m localized on the sites of a three-dimensional cubic lattice. On each site, the dipoles oscillate along the $x-$direction and are describe by pairs of conjugate variables $[x_i, p_j] = i\hbar\delta_{ij}$. The Hamiltonian for independent dipoles reads

$$H_0 = \sum_i H_{0,i} = \sum_i \frac{p_i^2}{2m} + \sum_i V_i(x_i) \qquad (1)$$

where $V_i(x_i) = V(x_i - R_i^x)$, is the on-site potential centered at the $i-$ the lattice site identified by the site vector

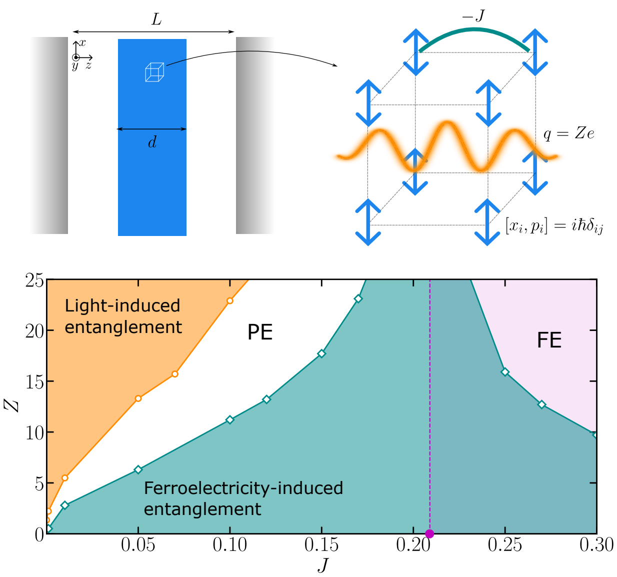

FIG. 1. Top: Schematic representation of the model of a cubic lattice of dipoles described by pairs of conjugate variables with nearest neighbor ferroelectric coupling ($-J$) and collective coupling with light in the cavity parametrized by the effective charge $q = Ze$, see Eq. 3. Bottom: Entanglement phase diagram in the $Z - J$ plane at $T = 0$. The coloured regions indicates the detection regions for entanglement between the dipoles induced, respectively, by the ferroelectric coupling (darkcyan) and the collective light-matter coupling (orange). The dot and the dashed line indicate the quantum phase transition between the paralectric (PE) and ferroelectric (FE) phase.

$\mathbf{R}_i$. We consider a quartic form of the potential

$$V(x) = m\omega_0^2 x^2 \left(\frac{1}{2} + k^2 \frac{m\omega_0}{\hbar} x^2\right) \tag{2}$$

where ω_0 is the harmonic frequency and k parametrizes the anharmonic part of the potential.

We supplement the model with two independent interactions: (i) an intrinsic nearest neighbor dipole-dipole interaction and (ii) the collective light-matter coupling between dipoles and the vacuum fluctuations of the electromagnetic fields, see Fig. 1. The interactions are parametrized, respectively, by a dimensionless ferroelectric coupling $J > 0$, and the effective charge of the dipoles $q = Ze$, being e the elementary charge. The full Hamiltonian becomes

$$H = \sum_i \frac{\left(p_i + Ze\hat{A}_i\right)^2}{2m} + V_i(x_i) - \frac{J}{2} m\omega_0^2 \sum_{\langle ij \rangle} x_i x_j + H_{em}. \tag{3}$$

Here, $\hat{A}_i = \sum_\mu A_{\mu,i}\left(a_\mu^\dagger + a_\mu\right)$ is the vector potential operator, with $a_\mu^\dagger$ and a_μ photon creation/annihilation operators, and $H_{em} = \sum_\mu \hbar\Omega_\mu a_\mu^\dagger a_\mu$ is the free photon Hamiltonian. Ω_μ is the frequency of the photon modes, with μ running over all the modes confined between two infinite parallel mirrors at distance L, details in App. B 3. The index i runs over all the N dipoles. In the following, we assume the thermodynamic limit $N \to \infty$, with the cubic lattice of finite thickness d and infinite dimensions in the x, y plane.

The two interactions act as independent sources of emergent collective behaviour. As a function of J, the model describes quantum criticality associated with ferroelectric order, i.e., $\langle x_i \rangle - R_i^x \neq 0$ [45–47]. At a finite $Z \neq 0$, the dipoles hybridize with light to form collective hybrid light-matter excitations dubbed as polaritons. The interplay between polariton formation and ferroelectricity has recently attracted a great deal of attention in relation to the so-called quantum paraelectrics, such as $SrTiO_3$ [34, 35], for which the light-matter coupling is particularly strong [48–52].

We define entanglement with respect to the local partitioning of the Hilbert space. A generic state ρ is said to be separable if it can be written as a convex combinations of product states

$$\rho = \sum_\alpha \lambda_\alpha \rho_\alpha^{(1)} \otimes \ldots \otimes \rho_\alpha^{(N)} \tag{4}$$

with $\lambda_\alpha \geq 0$, and $\sum_\alpha \lambda_\alpha = 1$. We denote the associated set as SEP. The extreme points of this set, with respect to convex combinations, are pure separable states, which take the form of product states, i.e., $|\psi\rangle = \bigotimes_i |\psi_i\rangle$. States that are not in SEP are said to be entangled.

To detect entanglement, we extend to the many-body case the entanglement criterion for continuous variables introduced by Duan *et al.* [53] and Simon [54] for two-particles systems. Given a collective operator O, not necessarily hermitian, and a state ρ, we define the fluctuation of O on ρ as $\Delta O_\rho^2 := \langle O^\dagger O\rangle_\rho - \langle O\rangle_\rho \langle O^\dagger\rangle_\rho$ where $\langle \cdot \rangle_\rho := \mathrm{Tr}[\cdot \rho]$ indicates the trace. If the state is the ground or a thermal state of a given Hamiltonian, the fluctuation can be extracted from response functions by fluctuation-dissipation theorem [55]

$$\Delta O_\rho^2 = \hbar \int_0^\infty d\omega \left(-\frac{1}{\pi}\mathrm{Im}\chi(\omega)\right) \coth\left(\frac{\beta\hbar\omega}{2}\right) \tag{5}$$

where $\chi(\omega) := \int dt e^{i\omega t}\chi(t)$, with $\chi(t) := -\frac{i}{\hbar}\theta(t)\langle[\mathcal{O}(t), \mathcal{O}^\dagger]\rangle_\rho$ and $\mathcal{O} := O - \langle O\rangle_\rho$ is the response function in the frequency domain, β is the inverse temperature, and the operators are time evolved (Heisenberg representation). We express the entanglement criterion in terms of dimensionless conjugate variables, $P_i := \frac{p_i}{\sqrt{\hbar m\omega_0}}$ and $X_i := x_i\sqrt{\frac{m\omega_0}{\hbar}}$. We define a set of collective position and momentum operators, $\mathbb{X} := \sum_{i=1}^N e^{i\varphi_i} X_i$ and $\mathbb{P} := \sum_{i=1}^N e^{i\vartheta_i} P_i$, where φ_i and ϑ_i are real phase factors. By using the uncertainty relations [56] $\Delta X_i^2 + \Delta P_i^2 \geq 1$, together with the concavity of the fluctuation, and the fact that the total fluctuation over a product state is the sum of the single-party fluctuations, we derive the minimum of the combined fluctuation $\Delta\mathbb{X}_\rho^2 + \Delta\mathbb{P}_\rho^2$ computed over all separable states (see App. A)

$$\min_{\rho\in\mathrm{SEP}} \Delta\mathbb{X}_\rho^2 + \Delta\mathbb{P}_\rho^2 = N. \tag{6}$$

Eq. (6) defines the lower bound of the entanglement criterion

$$\Delta\mathbb{X}_\rho^2 + \Delta\mathbb{P}_\rho^2 < N \quad \Rightarrow \quad \rho \notin \mathrm{SEP}. \tag{7}$$

In contrast to the QFI maximization, the criterion (7) detects entanglement by minimizing the combined fluctuations of two collective operators. To apply the criterion, we choose phase factors such that $[\mathbb{X}, \mathbb{P}] = \sum_i e^{i(\varphi_i+\vartheta_i)} = 0$. With this choice, it is always possible to define states with $\Delta\mathbb{X}_\rho^2 = \Delta\mathbb{P}_\rho^2 = 0$ such that, in principle, it is possible to fulfil the entanglement criterion by the simultaneous minimization of the uncertainties of both momentum and position collective variables. We interpret the criterion as the many-body generalization of the original EPR argument of the simultaneous determination of the center of mass and relative velocity for two entangled particles [31]. In the following, we refer to Eq. (7) as the EPR-criterion, and to $(\mathbb{X}, \mathbb{P})$ as a EPR-set of collective variables.

In a periodic lattice, such variables can be represented in terms of reciprocal space position and momentum variables, defined as $\mathbb{X}_{\mathbf{q}} := \frac{1}{\sqrt{N}} \sum_j e^{i\mathbf{q}\mathbf{R}_j} X_j$ and $\mathbb{P}_{\mathbf{q}} := \frac{1}{\sqrt{N}} \sum_j e^{i\mathbf{q}\mathbf{R}_j} P_j$, satisfying $[\mathbb{X}_{\mathbf{q}}, \mathbb{P}_{\mathbf{q}'}] = \delta_{\mathbf{q},-\mathbf{q}'}$ The entanglement criterion reduces, for $\mathbf{q} \neq -\mathbf{q}'$, to

$$\Delta\mathbb{X}_{\mathbf{q}\,\rho}^2 + \Delta\mathbb{P}_{\mathbf{q}'\,\rho}^2 < 1 \Rightarrow \quad \rho \notin \mathrm{SEP}. \tag{8}$$

Entanglement at the ferroelectric quantum critical point.— We first set $Z = 0$ and discuss entanglement detection in the ferroelectric model by considering the fully isotropic case $d \to \infty$, i.e., infinite thickness; see Fig. 1. We start from the harmonic case, $k = 0$ in Eq. (2). In this limit, the Hamiltonian is exactly diagonalized as $H = \sum_{\mathbf{q}} \hbar\omega_{\mathbf{q}} a_{\mathbf{q}}^\dagger a_{\mathbf{q}}$ with $\hbar\omega_{\mathbf{q}} = \hbar\omega_0 \left[1 - 2J\sum_{a=x,y,z}\cos(q_a a)\right]^{1/2}$ and $\left[a_{\mathbf{q}'}, a_{\mathbf{q}}^\dagger\right] = \delta_{\mathbf{q}\mathbf{q}'}$. $\mathbf{q} := (q_x, q_y, q_z)$ is a wave vector within the first Brillouin zone (BZ), and a is the lattice parameter. At $J = 0$, the spectrum is dispersionless, $\hbar\omega_{\mathbf{q}} = \hbar\omega_0$. At finite J, the frequency of the modes close to the BZ boundary, i.e., $\mathbf{q} = \boldsymbol{\pi} := \pi/a(1,1,1)$, increases (mode hardening). On the contrary, frequency of the modes close to the BZ center, i.e., $\mathbf{q} = \mathbf{0}$, decreases (mode softening). For $J \to 1/6$, the $\mathbf{q} = \mathbf{0}$ mode completely softens, i.e., $\omega_{\mathbf{q}=0}^2 \to 0$, signalling an instability towards a spectrum unbounded from below for $J > 1/6$.

The mode softening/hardening in different regions of the BZ reflects the different energetic costs of parallel/antiparallel configuration of dipoles. This observation guides the choice of the EPR-set $(\mathbb{X}_{\mathbf{q}}, \mathbb{P}_{\mathbf{q}'})$ for entanglement detection. In Fig. 2(a), we plot the mode squeezing parameter $\zeta_{\mathbf{q}} := \log\left(\Delta\mathbb{X}_{\mathbf{q}}^2/\Delta\mathbb{P}_{\mathbf{q}}^2\right)$ as a function of J and $\mathbf{q}$ along the $(1,1,1)$ direction of the BZ. For $k = 0$, the fluctuation reads $\Delta\mathbb{X}_{\mathbf{q}}^2 = \frac{1}{2\omega_{\mathbf{q}}}\coth\left(\frac{\beta\omega_{\mathbf{q}}}{2}\right)$ and

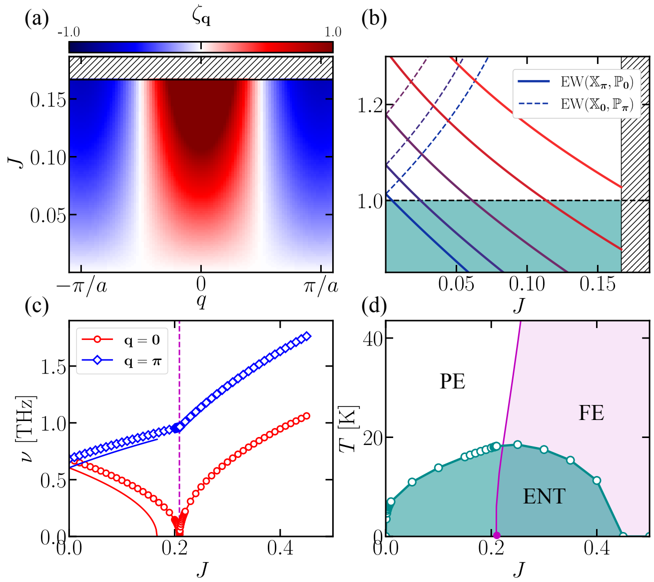

FIG. 2. Entanglement detection in the purely ferroelectric model. Top panels: harmonic potential, $k = 0$. The hatching in panels (a)-(b) highlights the instability of the model for $J > 1/6$. (a) Squeezing parameter as a function of $\mathbf{q} = q(1,1,1)$. $\zeta_{\mathbf{q}}$ is cut-off between -1 and 1 for illustration purposes. (b) Entanglement witnesses corresponding to the EPR-sets $(\mathbb{X}_{\boldsymbol{\pi}}, \mathbb{P}_{\mathbf{0}})$ (full lines) $(\mathbb{X}_{\mathbf{0}}, \mathbb{P}_{\boldsymbol{\pi}})$ and (dashed lines) for increasing temperature from $T_{\mathrm{cold}} \simeq 5.8$ K (blue) to $T_{\mathrm{hot}} \simeq 17.4$ K (red). Horizontal dashed line indicates the bound. Bottom panels: anharmonic potential, $k^2 = 0.05$. (c) Mode frequencies for $\mathbf{q} = \mathbf{0}$ (circles) and $\mathbf{q} = \boldsymbol{\pi}$ (diamonds) at $T = 0$ across the ferroelectric QCP. Full lines indicates the corresponding values for $k = 0$. (d) Phase diagram in the $J - T$ plane. The shaded region indicates the entanglement detection.

$\Delta\mathbb{P}_{\mathbf{q}}^2 = \frac{\omega_{\mathbf{q}}}{2}\coth\left(\frac{\beta\omega_{\mathbf{q}}}{2}\right)$. At $J = 0$, $\Delta\mathbb{X}_{\mathbf{q}}^2 = \Delta\mathbb{P}_{\mathbf{q}}^2 = 1/2$ and $\zeta_{\mathbf{q}} = 0$ for all $\mathbf{q}$. By increasing J, the softening (hardening) of the frequency $\omega_{\mathbf{q}}$ leads to a $\mathbf{q}-$selective squeezing: Modes at the BZ center become momentum squeezed, i.e., $\zeta_{\mathbf{q}} > 0$, with $\zeta_{\mathbf{q}=0} \to \infty$ for $J \to 1/6$. In contrast, modes at the BZ-boundary become position squeezed, i.e., $\zeta_{\mathbf{q}} < 0$. Therefore, position and momentum fluctuations are simultaneously minimized, see Eq. (8), by choosing $\mathbf{q}$ and $\mathbf{q}'$, respectively, at the boundary and the center of the BZ. In Fig. 2(b), we explicitly show the witnesses associated to the $(\mathbb{X}_{\mathbf{q}=\boldsymbol{\pi}}, \mathbb{P}_{\mathbf{q}'=\mathbf{0}})$ set as a function of J and temperature T. At $T = 0$, the EPR-criterion is fulfilled for any $J > 0$. By increasing temperature, the witness is enhanced by thermal fluctuations, and the criterion is fulfilled only for a critical coupling $J > J_\star(T)$ which monotonically increases with T. Eventually, after a threshold temperature no detection is possible in the entire $0 < J < 1/6$ range. At the same time, the witness for the complementary set $(\mathbb{X}_{\mathbf{q}=\mathbf{0}}, \mathbb{P}_{\mathbf{q}'=\boldsymbol{\pi}})$ monotonically increases with J and is never able to detect entanglement.

Turning on a finite $k \neq 0$, the soft mode instability

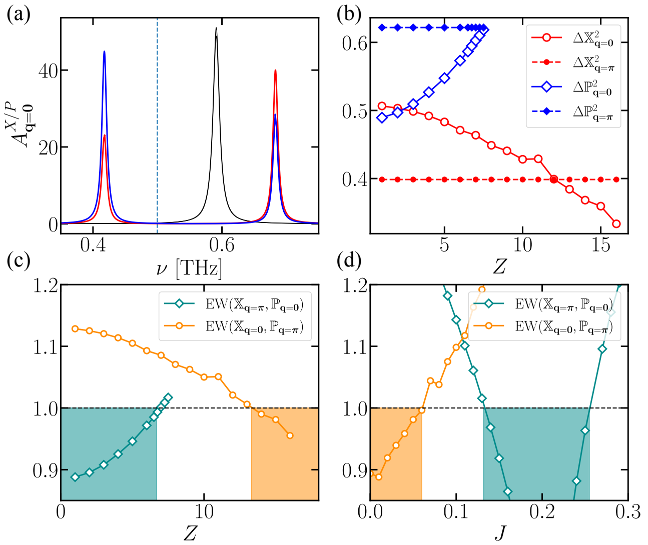

FIG. 3. Entanglement induced by the light-matter interaction Z. In all panels $T=0$. (a) Position (red) and momentum (blue) spectral functions for $J=0.05$ and $Z=4.0$, compared to the $Z=0$ case (thin black line). (b) Position and momentum fluctuations at $\mathbf{q}=\mathbf{0}$ as a function of Z, $J=0.05$. (c)-(d) Entanglement witnesses for the two sets $(\mathbb{X}_{\mathbf{q}=\boldsymbol{\pi}},\mathbb{P}_{\mathbf{q}=\mathbf{0}})$ and $(\mathbb{X}_{\mathbf{q}=\mathbf{0}},\mathbb{P}_{\mathbf{q}=\boldsymbol{\pi}})$ as a function of Z and fixed $J=0.05$, panel (c), and as a function of J and fixed $Z=15$.

evolves into a true ferroelectric quantum phase transition. We describe the phase transition by using a Gutzwiller variational ansatz [57, 58]. We find a quantum critical point (QCP) for $J_c \approx 0.209$ at the end of a second-order thermal transition line which separates the paraelectric (PE) and ferroelectric (FE) phases. We extract the $\mathbb{X}_\mathbf{q}$ and $\mathbb{P}_\mathbf{q}$ response functions, $\chi^X_\mathbf{q}(t) := -i\hbar\theta(t)\langle[\mathbb{X}_\mathbf{q}(t),\mathbb{X}_{-\mathbf{q}}]\rangle$ and $\chi^P_\mathbf{q}(t) := -i\hbar\theta(t)\langle[\mathbb{P}_\mathbf{q}(t),\mathbb{P}_{-\mathbf{q}}]\rangle$, from the non-equilibrium dynamics in the linear regime; see App. B for details. Using Eq. (5), we compute fluctuations and find a dome-like region around the QCP in which the set $(\mathbb{X}_{\mathbf{q}=\mathbf{0}},\mathbb{P}_{\mathbf{q}'=\boldsymbol{\pi}})$ detects entanglement, Fig. 2(d). The dome shape of the entanglement detections region is understood by observing that, at low temperatures, the fluctuations are well approximated by the quasi-harmonic expressions, $\Delta\mathbb{X}^2_\mathbf{q} \simeq 1/(2\omega_\mathbf{q})$ and $\Delta\mathbb{P}^2_\mathbf{q} \simeq \omega_\mathbf{q}/2$ with mode frequencies defined by averaging over the spectral functions $\omega_\mathbf{q} := \int_0^\infty d\omega A^X_\mathbf{q}(\omega)\omega/\int_0^\infty d\omega A^X_\mathbf{q}(\omega)$, with $A^X_\mathbf{q}(\omega) = -\mathrm{Im}\chi^X_\mathbf{q}(\omega)/\pi$. On the PE side of the transition, the $\mathbf{q}=\mathbf{0}$ and $\mathbf{q}=\boldsymbol{\pi}$ modes closely follow the harmonic results. By crossing the QCP, the $\mathbf{q}=\mathbf{0}$ mode undergoes a softening/hardening transition with a cusp-like singularity for $J=J_c$, whereas $\omega_{\boldsymbol{\pi}}$ monotonically increases with J, see Fig. 2(c). Therefore, the considerations made for the harmonic case on the PE side of the transition get mirrored to the FE side.

Light-induced entanglement. — We now consider $Z \neq 0$, and discuss detection of entanglement induced by the light-matter coupling. We compute light-dressed matter response functions by including, in the linear response, the dynamics of the self-sourced electromagnetic fields [59, 60]. To this extent, we set a finite $d = 0.2$ μm and split the site index $i=(n,z)$ into in-plane, n, and layer, $z=1,\ldots,N_z$, indices. We update the definition of the EPR-sets using $\mathbb{O}_{\mathbf{q}=\mathbf{0}} := \frac{1}{\sqrt{N_z}}\sum_z O_{\mathbf{q}_\parallel=\mathbf{0},z}$ and $\mathbb{O}_{\mathbf{q}=\boldsymbol{\pi}} = \frac{1}{\sqrt{N_z}}\sum_z(-1)^z O_{\mathbf{q}_\parallel=\boldsymbol{\pi},z}$, for $\mathbb{O}=\mathbb{X},\mathbb{P}$, and $O=X,P$ with $O_{\mathbf{q}_\parallel=\mathbf{0},z}$ the partial Fourier transform in the $x-y$ plane. Here, we fix the lattice spacing $a=0.5$ nm, leading to $N_z=400$ layers, and we set the cavity length to $L=300$ μm in order to have the fundamental cavity mode in the THz range. Different choices of parameters do not change the qualitative picture discussed below.

In Fig. 3(a) we report the light-dressed response functions for $\mathbb{X}_{\mathbf{q}=\mathbf{0}}$ and $\mathbb{P}_{\mathbf{q}=\mathbf{0}}$ at $T=0$, compared to the ones for $Z=0$. The finite $Z\neq 0$ splits the bare resonance into two polariton peaks separated by a gap. Due to the polariton formation, the homogeneous $\mathbf{q}=\mathbf{0}$ fluctuations, panel (b), get suppressed for the position channel and enhanced for the momentum one. This behaviour can be understood by using a toy model of two coupled oscillators with a minimal coupling-like interaction; see App. B 3 for details. On the contrary, the staggered fluctuations $\mathbb{X}_{\mathbf{q}=\boldsymbol{\pi}}$ and $\mathbb{P}_{\mathbf{q}=\boldsymbol{\pi}}$ are not affected at all by the light-matter coupling. This follows from energetic arguments: the frequencies of the dipoles and that of the electromagnetic waves with $|\mathbf{q}| \sim \frac{\pi}{a}$ are orders of magnitudes out of resonance. Therefore, light dressing is negligible for these modes.

In Fig. 3(c), where we report the witnesses for the two EPR-sets $(\mathbb{X}_{\mathbf{q}=\boldsymbol{\pi}},\mathbb{P}_{\mathbf{q}=\mathbf{0}})$ and $(\mathbb{X}_{\mathbf{q}=\mathbf{0}},\mathbb{P}_{\mathbf{q}=\boldsymbol{\pi}})$, as a function of Z and fixed J. By increasing Z, the set $(\mathbb{X}_{\mathbf{q}=\boldsymbol{\pi}},\mathbb{P}_{\mathbf{q}=\mathbf{0}})$, used to detect entanglement at the ferroelectric QCP, becomes entanglement-blind for $Z > Z_1$. The opposite happens for the $(\mathbb{X}_{\mathbf{q}=\mathbf{0}},\mathbb{P}_{\mathbf{q}=\boldsymbol{\pi}})$ set which, being entanglement-blind at $Z=0$, starts to detect entanglement for $Z > Z_2$. Upon inverting the roles of the $(\mathbb{X}_{\mathbf{q}=\mathbf{0}},\mathbb{P}_{\mathbf{q}=\boldsymbol{\pi}})$ and $(\mathbb{X}_{\mathbf{q}=\boldsymbol{\pi}},\mathbb{P}_{\mathbf{q}=\mathbf{0}})$ sets, the analogous behaviour is observed by increasing J at fixed Z, see Fig. 3(d).

Discussion.— We summarize the entanglement detection in the phase diagram of Fig. 1. Remarkably, the detection region of the $(\mathbb{X}_{\mathbf{q}=\mathbf{0}},\mathbb{P}_{\mathbf{q}=\boldsymbol{\pi}})$ set extends down to $J\to 0$, showing that the light-matter coupling act as an independent source of entanglement which is not related to the ferroelectric one. By increasing J, the light-induced entanglement detection region is pushed to higher values of Z whereas the presence of the QCP protects the ferroelectric entanglement. From a physical perspective, we can understand these results by noticing that photons act as a thermal bath on the dipoles [61], possibly causing a degradation of the entanglement in the system. At the same time, however, due to the strong light-matter coupling, entanglement gets transferred from the photon bath to the system leading to an entanglement of a different origin. Indeed, it is known that the vacuum of a quantum field is an entangled state [62, 63] and such entanglement can be transferred, through the mechanism of entanglement harvesting [63–65], to probe two-level detectors as well as more complex physical systems, such as ions in a trap and cold atoms [66, 67]. In this respect, our results show a concrete example of entanglement harvesting occurring in the equilibrium state of a quantum material.

The starkly different behaviour of the witnesses associated with the detected entanglement highlights the competing nature of the two types of emergent behaviours. This can be understood by considering the different symmetry breaking triggered by large position and momentum fluctuations. As seen before, position fluctuations diverge at the ferroelectric QCP. On the contrary, the divergence of momentum fluctuations would indicate the breaking of time-reversal symmetry rather than ferroelectricity [68, 69]. Even though this symmetry breaking never happens in our model, the large momentum fluctuations in the light-induced detection region indicate that such a competing order is able to sensibly modify the nature of the detected entanglement around the ferroelectric QCP. In all these considerations, however, one should keep in mind that the failure to fulfill Eq. (7) does not necessarily mean that the state is separable.

In summary, we investigated entanglement detection in a model of a interacting dipoles in the presence of competing orders, linked, respectively, to the ferroelectric QCP and to the collective light-matter coupling. We used criteria based on the simultaneous suppression of collective fluctuations in position and momentum. Collective fluctuations can be extracted from dynamical susceptibilities or directly assessed through the measurement of the corresponding collective variables [70, 71]. Entanglement is witnessed when the combined value of the fluctuations falls below a threshold, determined by canonical commutation relations.

Our findings directly point to the investigation of entanglement in quantum paraelectrics exhibiting significant polariton splitting. The detection scheme in combination with the possibility of tuning polaritons [72, 73] represent a powerful tool for the control of the collective entanglement in these systems. The construction of different witnesses with different variables and wave vectors can reveal entanglement of different origin, which is not necessarily tied to spontaneous symmetry breaking, potentially unlocking the detection in a broad range of quantum materials.

Acknowledgements.— The authors thank Giuseppe Vitagliano, Matteo Mitrano and Marco Polini for useful discussions. G.M. acknowledges support from the MUR - Italian Minister of University and Research - under the "Rita Levi-Montalcini" program, and from the Swiss National Science Foundation through an AMBIZIONE grant (#PZ00P2_186145). C.B. acknowledges support from the Austrian Science Fund (FWF) through projects ZK 3 (Zukunftskolleg) and F 7113 (BeyondC).

[1] A. Osterloh, L. Amico, G. Falci, and R. Fazio, Nature **416**, 608 (2002).
[2] J. Vidal, G. Palacios, and R. Mosseri, Phys. Rev. A **69**, 022107 (2004).
[3] P. Hauke, M. Heyl, L. Tagliacozzo, and P. Zoller, Nature Physics **12**, 778 (2016).
[4] T. J. Osborne and M. A. Nielsen, Phys. Rev. A **66**, 032110 (2002).
[5] H.-C. Jiang, Z. Wang, and L. Balents, Nature Physics **8**, 902 (2012).
[6] L. Savary and L. Balents, Reports on Progress in Physics **80**, 016502 (2016).
[7] C. Walsh, M. Charlebois, P. Sémon, G. Sordi, and A.-M. S. Tremblay, Proceedings of the National Academy of Sciences **118** (2021), 10.1073/pnas.2104114118.
[8] G. Bellomia, C. Mejuto-Zaera, M. Capone, and A. Amaricci, (2023), arXiv:2308.13706 [cond-mat.str-el].
[9] F. Giustino, J. H. Lee, F. Trier, M. Bibes, S. M. Winter, R. Valentí, Y.-W. Son, L. Taillefer, C. Heil, A. I. Figueroa, B. Placais, Q. Wu, O. V. Yazyev, E. P. A. M. Bakkers, J. Nygard, P. Forn-Díaz, S. D. Franceschi, J. W. McIver, L. E. F. F. Torres, T. Low, A. Kumar, R. Galceran, S. O. Valenzuela, M. V. Costache, A. Manchon, E.-A. Kim, G. R. Schleder, A. Fazzio, and S. Roche, Journal of Physics: Materials **3**, 042006 (2021).
[10] D. N. Basov, R. D. Averitt, and D. Hsieh, Nature Materials **16**, 1077 (2017).
[11] O. Gühne and G. Tóth, Physics Reports **474**, 1 (2009).
[12] R. Horodecki, P. Horodecki, M. Horodecki, and K. Horodecki, Rev. Mod. Phys. **81**, 865 (2009).
[13] N. Friis, G. Vitagliano, M. Malik, and M. Huber, Nature Reviews Physics **1**, 72 (2019).
[14] C. W. Helstrom, Journal of Statistical Physics **1**, 231 (1969).
[15] S. L. Braunstein and C. M. Caves, Phys. Rev. Lett. **72**, 3439 (1994).
[16] L. Pezzé and A. Smerzi, Phys. Rev. Lett. **102**, 100401 (2009).
[17] P. Hyllus, W. Laskowski, R. Krischek, C. Schwemmer, W. Wieczorek, H. Weinfurter, L. Pezzé, and A. Smerzi, Phys. Rev. A **85**, 022321 (2012).
[18] G. Tóth and I. Apellaniz, Journal of Physics A: Mathematical and Theoretical **47**, 424006 (2014).
[19] M. Wieśniak, V. Vedral, and Časlav Brukner, New Journal of Physics **7**, 258 (2005).
[20] G. Mathew, S. L. L. Silva, A. Jain, A. Mohan, D. T. Adroja, V. G. Sakai, C. V. Tomy, A. Banerjee, R. Goreti, A. V. N., R. Singh, and D. Jaiswal-Nagar, Phys. Rev. Res. **2**, 043329 (2020).
[21] P. Laurell, A. Scheie, C. J. Mukherjee, M. M. Koza, M. Enderle, Z. Tylczynski, S. Okamoto, R. Coldea, D. A. Tennant, and G. Alvarez, Phys. Rev. Lett. **127**, 037201 (2021).
[22] D. R. Baykusheva, M. H. Kalthoff, D. Hofmann, M. Claassen, D. M. Kennes, M. A. Sentef, and M. Mitrano, Phys. Rev. Lett. **130**, 106902 (2023).
[23] J. Hales, U. Bajpai, T. Liu, D. R. Baykusheva, M. Li, M. Mitrano, and Y. Wang, Nature Communications **14**,

3512 (2023).
[24] F. Mazza, S. Biswas, X. Yan, A. Prokofiev, P. Steffens, Q. Si, F. F. Assaad, and S. Paschen, (2024), arXiv:2403.12779 [cond-mat.str-el].
[25] M. Gessner, L. Pezzè, and A. Smerzi, Phys. Rev. A **94**, 020101 (2016).
[26] T. Ren, Y. Shen, S. F. R. TenHuisen, J. Sears, W. He, M. H. Upton, D. Casa, P. Becker, M. Mitrano, M. P. M. Dean, and R. M. Konik, (2024), arXiv:2404.05850 [cond-mat.str-el].
[27] A. Sorensen, L.-M. Duan, J. I. Cirac, and P. Zoller, Nature **409**, 63 (2001).
[28] A. S. Sorensen and K. Molmer, Phys. Rev. Lett. **86**, 4431 (2001).
[29] G. Tóth, C. Knapp, O. Gühne, and H. J. Briegel, Phys. Rev. A **79**, 042334 (2009).
[30] G. Vitagliano, P. Hyllus, I. n. L. Egusquiza, and G. Tóth, Phys. Rev. Lett. **107**, 240502 (2011).
[31] A. Einstein, B. Podolsky, and N. Rosen, Phys. Rev. **47**, 777 (1935).
[32] M. D. Reid, Phys. Rev. A **40**, 913 (1989).
[33] M. D. Reid, P. D. Drummond, W. P. Bowen, E. G. Cavalcanti, P. K. Lam, H. A. Bachor, U. L. Andersen, and G. Leuchs, Rev. Mod. Phys. **81**, 1727 (2009).
[34] K. A. Müller and H. Burkard, Phys. Rev. B **19**, 3593 (1979).
[35] S. E. Rowley, L. J. Spalek, R. P. Smith, M. P. M. Dean, M. Itoh, J. F. Scott, G. G. Lonzarich, and S. S. Saxena, Nature Physics **10**, 367 (2014).
[36] C. W. Rischau, X. Lin, C. P. Grams, D. Finck, S. Harms, J. Engelmayer, T. Lorenz, Y. Gallais, B. Fauqué, J. Hemberger, and K. Behnia, Nature Physics **13**, 643 (2017).
[37] A. Narayan, A. Cano, A. V. Balatsky, and N. A. Spaldin, Nature Materials **18**, 223 (2019).
[38] F. J. Garcia-Vidal, C. Ciuti, and T. W. Ebbesen, Science **373** (2021), 10.1126/science.abd0336.
[39] F. Schlawin, D. M. Kennes, and M. A. Sentef, Applied Physics Reviews **9**, 011312 (2022), https://pubs.aip.org/aip/apr/article-pdf/doi/10.1063/5.0083825/19819541/011312_1_online.pdf.
[40] G. Jarc, S. Y. Mathengattil, A. Montanaro, F. Giusti, E. M. Rigoni, R. Sergo, F. Fassioli, S. Winnerl, S. Dal Zilio, D. Mihailovic, P. Prelovšek, M. Eckstein, and D. Fausti, Nature **622**, 487 (2023).
[41] F. Appugliese, J. Enkner, G. L. Paravicini-Bagliani, M. Beck, C. Reichl, W. Wegscheider, G. Scalari, C. Ciuti, and J. Faist, Science **375**, 1030 (2022).
[42] G. Mazza and A. Georges, Phys. Rev. Lett. **122**, 017401 (2019).
[43] G. M. Andolina, F. M. D. Pellegrino, V. Giovannetti, A. H. MacDonald, and M. Polini, Phys. Rev. B **100**, 121109 (2019).
[44] G. Passetti, C. J. Eckhardt, M. A. Sentef, and D. M. Kennes, Phys. Rev. Lett. **131**, 023601 (2023).
[45] N. S. Gillis and T. R. Koehler, Phys. Rev. B **9**, 3806 (1974).
[46] L. Pálová, P. Chandra, and P. Coleman, Phys. Rev. B **79**, 075101 (2009).
[47] R. Roussev and A. J. Millis, Phys. Rev. B **67**, 014105 (2003).
[48] Y. Ashida, A. Imamoglu, J. Faist, D. Jaksch, A. Cavalleri, and E. Demler, Phys. Rev. X **10**, 041027 (2020).
[49] D. Shin, S. Latini, C. Schäfer, S. A. Sato, U. De Giovannini, H. Hübener, and A. Rubio, Phys. Rev. B **104**, L060103 (2021).
[50] P. Pilar, D. De Bernardis, and P. Rabl, Quantum **4**, 335 (2020).
[51] S. Latini, D. Shin, S. A. Sato, C. Schäfer, U. D. Giovannini, H. Hübener, and A. Rubio, Proceedings of the National Academy of Sciences **118**, e2105618118 (2021).
[52] J. B. Curtis, M. H. Michael, and E. Demler, Phys. Rev. Res. **5**, 043118 (2023).
[53] L.-M. Duan, G. Giedke, J. I. Cirac, and P. Zoller, Phys. Rev. Lett. **84**, 2722 (2000).
[54] R. Simon, Phys. Rev. Lett. **84**, 2726 (2000).
[55] M. Fabrizio, *A Course in Quantum Many-Body Theory* (Springer Cham, 2022).
[56] P. Busch, P. Lahti, and R. F. Werner, Rev. Mod. Phys. **86**, 1261 (2014).
[57] W. Krauth, M. Caffarel, and J.-P. Bouchaud, Phys. Rev. B **45**, 3137 (1992).
[58] F. Caleffi, M. Capone, C. Menotti, I. Carusotto, and A. Recati, Phys. Rev. Res. **2**, 033276 (2020).
[59] I. Amelio, L. Korosec, I. Carusotto, and G. Mazza, Phys. Rev. B **104**, 235120 (2021).
[60] J. Flick, D. M. Welakuh, M. Ruggenthaler, H. Appel, and A. Rubio, ACS Photonics **6**, 2757 (2019).
[61] F. Fassioli, J. Faist, M. Eckstein, and D. Fausti, (2024), arXiv:2403.00851 [physics.optics].
[62] S. J. Summers and R. Werner, Physics Letters A **110**, 257 (1985).
[63] B. Reznik, Foundations of Physics **33**, 167 (2003).
[64] B. Reznik, A. Retzker, and J. Silman, Phys. Rev. A **71**, 042104 (2005).
[65] G. Salton, R. B. Mann, and N. C. Menicucci, New Journal of Physics **17**, 035001 (2015).
[66] A. Retzker, J. I. Cirac, and B. Reznik, Phys. Rev. Lett. **94**, 050504 (2005).
[67] H. T. Ng and K. Burnett, New Journal of Physics **10**, 123014 (2008).
[68] G. Mazza and M. Polini, Phys. Rev. B **108**, L241107 (2023).
[69] A. Mercurio, G. M. Andolina, F. M. D. Pellegrino, O. Di Stefano, P. Jarillo-Herrero, C. Felser, F. H. L. Koppens, S. Savasta, and M. Polini, Phys. Rev. Res. **6**, 013303 (2024).
[70] C. Meng, G. A. Brawley, S. Khademi, E. M. Bridge, J. S. Bennett, and W. P. Bowen, Science Advances **8** (2022), 10.1126/sciadv.abm7585.
[71] M. Esposito, K. Titimbo, K. Zimmermann, F. Giusti, F. Randi, D. Boschetto, F. Parmigiani, R. Floreanini, F. Benatti, and D. Fausti, Nature communications **6**, 10249 (2015).
[72] D. N. Basov, M. M. Fogler, and F. J. García De Abajo, Science (80-.). **354** (2016), 10.1126/science.aag1992.
[73] Y. Zhou, A. Waelchli, M. Boselli, I. Crassee, A. Bercher, W. Luo, J. Duan, J. L. M. van Mechelen, D. van der Marel, J. Teyssier, C. W. Rischau, L. Korosec, S. Gariglio, J.-M. Triscone, and A. B. Kuzmenko, Nature Communications **14**, 7686 (2023).
[74] H. F. Hofmann and S. Takeuchi, Phys. Rev. A **68**, 032103 (2003).

Appendix A: Entanglement criteria

To make our discussion about entanglement self-contained, we provide all the details of the derivation of the entanglement criteria presented in the main text, together with the original references.
Given an operator A, its fluctuation on a quantum state ρ is defined as

$$\Delta A^2_\rho := \langle (A^\dagger - \langle A^\dagger\rangle_\rho)(A - \langle A\rangle_\rho)\rangle_\rho = \langle A^\dagger A\rangle_\rho - \langle A^\dagger\rangle_\rho \langle A\rangle_\rho. \tag{A1}$$

Notice that, since the operator A is, in general, not Hermitian, we explicitly avoid calling this object a variance. We also define the symbol $\Delta A_\rho := \sqrt{\Delta A^2_\rho}$. Notice that, even if A is not an Hermitian operator, as long as it is normal, i.e., $[A^\dagger, A] = 0$, the interpretation of $\langle A\rangle$ as an expectation value still holds. In fact, for normal operators the spectral theorem holds: we can still diagonalize it (with complex eigenvalues) and thus make sense of measurements of it. This is the case we consider here.
One can show that the fluctuation is a concave function of the quantum state, namely, for $\rho = \sum_i \lambda_i \rho_i$, with $\{\rho_i\}_i$ quantum states and coefficients $\lambda_i \geq 0$ and $\sum_i \lambda_i = 1$, we have

$$\Delta A^2_\rho \geq \sum_i \lambda_i \Delta A^2_{\rho_i}. \tag{A2}$$

This can be easily shown, with a slight modification of the argument in [74], as follows

$$\begin{aligned}
\Delta A^2_\rho &= \mathrm{tr}[(A^\dagger - \langle A^\dagger\rangle_\rho)(A - \langle A\rangle_\rho)\rho] = \sum_i \lambda_i \,\mathrm{tr}[(A^\dagger - \langle A^\dagger\rangle_\rho)(A - \langle A\rangle_\rho)\rho_i] \\
&= \sum_i \lambda_i \left(\mathrm{tr}[(A^\dagger - \langle A^\dagger\rangle_\rho)(A - \langle A\rangle_\rho)\rho_i] + \langle A^\dagger\rangle_{\rho_i}\langle A\rangle_{\rho_i} - \langle A^\dagger\rangle_{\rho_i}\langle A\rangle_{\rho_i}\right) \\
&= \sum_i \lambda_i \left(\mathrm{tr}[(A^\dagger A - \langle A^\dagger\rangle_{\rho_i}\langle A\rangle_{\rho_i})\rho_i] + \langle A^\dagger\rangle_{\rho_i}\langle A\rangle_{\rho_i} - \langle A^\dagger\rangle_{\rho}\langle A\rangle_{\rho_i} - \langle A^\dagger\rangle_{\rho_i}\langle A\rangle_{\rho} + \langle A^\dagger\rangle_{\rho}\langle A\rangle_{\rho}\right) \\
&= \sum_i \lambda_i \left(\Delta A^2_{\rho_i} + |\langle A\rangle_\rho - \langle A\rangle_{\rho_i}|^2\right) \\
&\geq \sum_i \lambda_i \Delta A^2_{\rho_i}.
\end{aligned} \tag{A3}$$

The concavity property implies that the minimum is achieved on extreme states, i.e., pure. Now consider an operator A on a tensor product $\mathcal{H} = \bigotimes_i \mathcal{H}_i$ defined as a sum of local operators $A = \sum_i \tilde{a}_i$, where $\tilde{a}_i$ is an operator acting on the Hilbert space $\mathcal{H}_i$ and identity everywhere else, e.g., $\tilde{a}_1 = a_1 \otimes \mathbb{1} \otimes \ldots \otimes \mathbb{1}$. Its fluctuation on a product state $\rho = \bigotimes_i \rho_i$ is given by

$$\begin{aligned}
\Delta A^2_\rho &= \sum_{ij} \mathrm{tr}[\tilde{a}_i^\dagger \tilde{a}_j \bigotimes_k \rho_k] - \sum_{i,j} \mathrm{tr}[a_i^\dagger \rho_i]\,\mathrm{tr}[a_j \rho_j] \\
&= \sum_{i\neq j} \Big(\mathrm{tr}[a_i^\dagger \rho_i]\,\mathrm{tr}[a_j\rho_j] - \mathrm{tr}[a_i^\dagger \rho_i]\,\mathrm{tr}[a_j\rho_j]\Big) + \sum_i \Big(\mathrm{tr}[a_i^\dagger a_i \rho_i] - \mathrm{tr}[a_i^\dagger \rho_i]\,\mathrm{tr}[a_i\rho_i]\Big) \\
&= \sum_i (\Delta a_i^2)_{\rho_i}.
\end{aligned} \tag{A4}$$

Finally, combining Eq. (A2), the fact that all separable states can be written as a convex mixture of pure product states, and Eq. (A4), we have that for any collective variable $A = \sum_i \tilde{a}_i$ defined as above

$$\min_{\rho\in\mathrm{SEP}} \Delta A^2_\rho = \min_{\psi\in\mathrm{PPROD}} \Delta A^2_\psi = \min_{\{\psi_i\}_i} \sum_i (\Delta a_i^2)_{\psi_i}, \tag{A5}$$

where SEP denotes the set of separable states, i.e., states of the form $\rho = \sum_i \lambda_i \sigma_1^{(i)} \otimes \ldots \otimes \sigma_n^{(i)}$, for $\lambda_i \geq 0, \sum_i \lambda_i = 1$, PPROD the set of pure product states, i.e., $|\psi\rangle = \bigotimes_i |\psi_i\rangle$, ΔA^2_ψ denotes the fluctuation of A on a global pure state $|\psi\rangle$, and $(\Delta a_i^2)_{\psi_i}$ the fluctuation of the local observable a_i on a local pure state $|\psi_i\rangle$.
We recall the uncertainty relation [56]

$$\Delta X \Delta Y \geq \frac{1}{2}|\langle [X, Y]\rangle| \tag{A6}$$

which combined with the inequality $(a-b)^2 = a^2 + b^2 - 2ab \geq 0$, for $a, b \in \mathbb{R}$, gives

$$\Delta X^2 + \Delta Y^2 \geq 2\Delta X \Delta Y \geq |\langle [X, Y] \rangle|. \tag{A7}$$

Now, applying Eq. (A5) together with Eq. (A7) for the sum of two collective variables, i.e., $A = \sum_i \tilde{a}_i$ and $B = \sum_i \tilde{b}_i$, we have

$$\min_{\rho \in \mathrm{SEP}} (\Delta A_\rho^2 + \Delta B_\rho^2) = \min_{\{\psi_i\}_i} \sum_i \left[(\Delta a_i^2)_{\psi_i} + (\Delta b_i^2)_{\psi_i} \right] \geq \sum_i |\langle [a_i, b_i] \rangle_{\psi_i}|. \tag{A8}$$

This equation gives Eq. (6) for the choice $a_j = e^{i\phi_j} x_j$ and $b_j = e^{i\theta_j} p_j$.

Appendix B: Model of interacting dipoles

1. Linear response dynamics

In this section we detail the calculation of the response functions using the time-dependent Gutzwiller ansatz. Our goal is to computed the response functions at wave-vector $\mathbf{q}$, defined as

$$\chi_{\mathbf{q}}^O(t) = -i\theta(t) \langle [\mathbb{O}_{\mathbf{q}}, \mathbb{O}_{\mathbf{q}}^\dagger] \rangle = -i\theta(t) \langle [\mathbb{O}_{\mathbf{q}}, \mathbb{O}_{-\mathbf{q}}] \rangle \tag{B1}$$

for $\mathbb{O} = \mathbb{X}, \mathbb{P}$, where $\mathbb{O}_{\mathbf{q}}^\dagger = \mathbb{O}_{-\mathbf{q}}$. By linear response theory, the response functions can be extracted from the unitary dynamics with a time-dependent Hamiltonian supplemented by a small perturbation field $\lambda(t)$. By defining the Hermitean operators

$$\mathbb{O}_{\mathbf{q}+} := \mathbb{O}_{\mathbf{q}} + \mathbb{O}_{\mathbf{q}}^\dagger \qquad\qquad \mathbb{O}_{\mathbf{q}-} := -i \left(\mathbb{O}_{\mathbf{q}} - \mathbb{O}_{\mathbf{q}}^\dagger \right), \tag{B2}$$

we introduce the **q**- and time-dependent Hamiltonians

$$H_{\mathbf{q}\pm}(t) = H + \lambda(t) \mathbb{O}_{\mathbf{q}\pm}, \tag{B3}$$

the corresponding time-evolved states

$$\rho_{\mathbf{q},\pm}(t) := e^{i\int_0^t dt' H_{\mathbf{q}\pm}(t')} \rho_0 e^{-i\int_0^t dt' H_{\mathbf{q}\pm}(t')}. \tag{B4}$$

We therefore define the four expectation values with functional dependence on the perturbation $\lambda(t)$,

$$O_{\mathbf{q}}^{\pm\pm}(t) = O_{\mathbf{q}}^{\pm\pm}[\lambda(t)] = \mathrm{Tr}\left[\rho_{\mathbf{q},\pm}(t) \mathbb{O}_{\mathbf{q}\pm} \right]. \tag{B5}$$

The response functions encode the functional dependence at linear order in the perturbation $\lambda(t)$ as

$$O_{\mathbf{q}}^{\pm\pm}(t) = \int_{-\infty}^{+\infty} dt' \chi_{\mathbf{q}}^{\pm\pm}(t-t') \lambda(t') \tag{B6}$$

with

$$\chi_{\mathbf{q}}^{\pm\pm}(t-t') = -i\theta(t-t') \langle [\mathbb{O}_{\mathbf{q}\pm}(t), \mathbb{O}_{\mathbf{q},\pm}(t')] \rangle. \tag{B7}$$

The knowledge of the time-dependent expectation values $O_{\mathbf{q}}^{\pm\pm}(t)$ allows the determination of the response functions, Eq. (B7), by Fourier transform

$$O_{\mathbf{q}}^{\pm\pm}(\omega) = \chi_{\mathbf{q}}^{\pm\pm}(\omega) \lambda(\omega). \tag{B8}$$

The response function, Eq. (B1), is therefore obtained as

$$\chi_{\mathbf{q}}^O(\omega) = \frac{1}{4} \left[\chi_{\mathbf{q}}^{++}(\omega) + \chi_{\mathbf{q}}^{--}(\omega) - i(\chi_{\mathbf{q}}^{+-}(\omega) - \chi_{\mathbf{q}}^{-+}(\omega)) \right] \tag{B9}$$

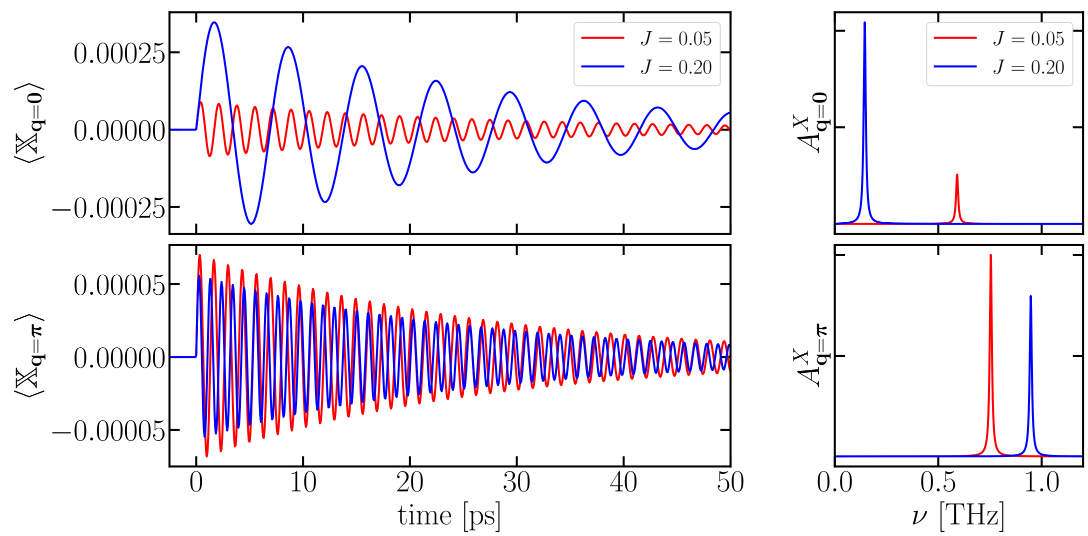

FIG. 4. Left panels: Linear response dynamics of the position operator for $\mathbf{q} == 0$ (top) and $\mathbf{q} = \boldsymbol{\pi}$ (bottom) and increasing value of J. Right panels: Position response functions obtained by Fourier transform of the time signals.

2. Gutzwiller dynamics

To study the dynamics of the interacting model of dipoles we use a Gutzwiller single-site ansatz

$$\rho(t) = \bigotimes_i \rho_i(t)$$

where $\rho_i(t)$ is a state defined on the Hilbert space of the dipole at site i, which evolves with an effective single-site Hamiltonian

$$H_i(t) = H_{0,i}(t) - x_i J_{eff,i}(t) \tag{B10}$$

with $J_{eff,i}(t) = Jm\omega_0^2 \sum_{\langle j \rangle} \mathrm{Tr}\left(\rho_j(t) x_j\right)$ where the sum over j is restricted to the nearest neighbour sites of i. In the static limit, this procedure corresponds to the static mean-field ansatz which describes the spontaneous symmetry breaking at mean-field level. In the time-dependent case, the method is able to capture quantum fluctuations on top of the static mean-field. It can be shown that the dynamics is exact in the two limits $\frac{k}{J} \to 0$ (harmonic limit) and $\frac{k}{J} \to \infty$ (atomic limit), where k and J are, respectively, the on-site and nearest-neighbor coupling constants in Eq. (1).

In order to study the dynamics, we represent the states $\rho_i(t)$ a local local basis sets containing $N_i = 10$ eigenstates and checked convergence with respect to N_i. We used a gaussian perturbation $\lambda(t) = \lambda_0 e^{-\frac{t^2}{\tau^2}}$ with $\lambda_0 = 10^{-3}\hbar\omega_0$ and $\tau = 10^{-5}$ ps. In Fig. 4 we show examples of linear response dynamics for the position operator with $\mathbf{q} = \mathbf{0}$ and the $\mathbf{q} = \boldsymbol{\pi}$ wavevectors. We extract the response functions by evaluating the Fourier transform over a time window of 500 ps. In the dynamics, we included a small damping which ensures convergence of the Fourier integrals in the considered time window.

3. Light-dressed response functions

In this section we show details of the calculation of the light-dressed response functions. We first write the full Hamiltonian of the dipoles interacting with the photon degrees of freedom.

$$H = \sum_\mu \hbar\Omega_\mu a^\dagger_\mu a_\mu + \sum_i \frac{1}{2m}\left(p_i + Ze\hat{A}_x(x_i)\right)^2 + V_i(x_i) - Jm\omega_0^2 x^2 \left(\frac{1}{2} + k^2 \frac{m\omega_0}{\hbar} x^2\right) \tag{B11}$$

Here, $\hat{A}_x(x_i)$ is the $x-$component of the vector potential operator computed at the position of the point-like dipole. Specifically, starting from the full vector potential operator defined in all the points of the three-dimensional space,

$$\hat{\mathbf{A}}(\mathbf{x}) = \hat{\mathbf{A}}(x,y,z) = \boldsymbol{x}\hat{A}_x(x,y,z) + \boldsymbol{y}\hat{A}_y(x,y,z) + \boldsymbol{z}\hat{A}_z(x,y,z), \tag{B12}$$

the operator $\hat{A}_x(x_i)$ is defined as

$$\hat{A}_x(x_i) := \int dxdydz A_x(x,y,z)\delta(x-x_i)\delta(y-R_i^y)\delta(z-R_i^z). \tag{B13}$$

Notice that the $y-$ and $z-$ components of the vector potential do not enter the Hamiltonian as the dipoles oscillates only along the $x-$direction. The full vector potential quantized in the volume of the cavity reads

$$\hat{\mathbf{A}}(\mathbf{x}) = \sum_\mu A_\mu \left(\mathbf{u}_\mu(\mathbf{x})a_\mu + \mathbf{u}_\mu^*(\mathbf{x})a_\mu^\dagger\right) \qquad A_\mu = \sqrt{\frac{\hbar^2}{2\epsilon_0\Omega_\mu V}} \qquad \Omega_\mu = \hbar c|\mathbf{q}_\mu| \tag{B14}$$

where the mode functions form a complete set of functions which satisfy the wave equation and the divergence-less condition

$$\vec{\nabla}^2\mathbf{u}_\mu + \mathbf{q}_\mu^2\mathbf{u}_\mu = 0 \qquad \nabla\cdot\mathbf{u}_\mu = 0 \qquad \frac{1}{V}\int d\mathbf{x}\ \mathbf{u}_\mu^*\cdot\mathbf{u}_{\mu'} = \delta_{\mu\mu'}, \tag{B15}$$

with boundary conditions set by perfectly reflecting mirrors.
We supplement the Hamiltonian with the linear response perturbation, as in Eq. (B3)

$$H_{\mathbf{q}\pm}(t) = \sum_\mu \hbar\Omega_\mu a_\mu^\dagger a_\mu + \sum_i \frac{1}{2m}\left(p_i + Ze\hat{A}_x(x_i)\right)^2 + V_i(x_i) - Jm\omega_0^2x^2\left(\frac{1}{2} + k^2\frac{m\omega_0}{\hbar}x^2\right) + \lambda(t)\mathbb{O}_{\mathbf{q}\pm}. \tag{B16}$$

We therefore follow Ref. [59] and write the dynamics as the coupled dynamics of dipoles in the presence of fields whose evolution is governed by the Maxwell equations with the dipoles acting as sources of currents. Specifically, density matrix of the dipoles evolves with the Hamiltonian

$$H_{\mathbf{q}\pm}[A,t] = \sum_i \frac{1}{2m}\left(p_i + ZeA_x(x_i)\right)^2 + V_i(x_i) - Jm\omega_0^2x^2\left(\frac{1}{2} + k^2\frac{m\omega_0}{\hbar}x^2\right) + \lambda(t)\mathbb{O}_{\mathbf{q}\pm}. \tag{B17}$$

$$i\hbar\partial_t\rho_{\mathbf{q}\pm} = \left[H_{\mathbf{q}\pm}(t), \rho_{\mathbf{q}\pm}\right]. \tag{B18}$$

where the field entering Eq. (B17) satisfy

$$-\nabla^2 A_x(\mathbf{x}) - \frac{1}{c^2}\frac{\partial^2 A_x(\mathbf{x})}{\partial t^2} = \mu_0 J_x(\mathbf{x}). \tag{B19}$$

In Eq. (B19), the current density reads

$$J_x(\mathbf{x}) = \sum_i \mathrm{Tr}\left(\rho_{\mathbf{q}\pm}(t)\hat{J}_{x,i}(\mathbf{x})\right),$$

being $\hat{J}_{x,i}(\mathbf{x})$ the current density operator associated with the i-th dipole

$$\hat{J}_{x,i}(\mathbf{x}) = \hat{J}_{x,i}(x,y,z) = \frac{Ze}{m}\left(p_i + Ze\hat{A}_x(x_i)\right)\delta(x-x_i)\delta(y-R_i^y)\delta(z-R_i^z), \tag{B20}$$

Eventually, the computation of the light-dressed response functions reduces to the coupled dynamics of dipoles in the presence of self-sourced fields, Eqs. (B18)-(B19). The dynamics of the dipoles is solved using the same method described above. We solve the wave-equation of the field, Eq. (B19), by expanding the field on the quantized mode in the cavity, Eq. (B15). In practice, we average the point-like current density over a volume a^3 around each lattice site and assume the vector potential constant within each volume a^3.

$$J_x(\mathbf{x}) = \sum_i \frac{1}{a^3}\mathrm{Tr}\left(\rho(t)\hat{J}_i^x\right)\theta\left(|x-R_i^x| - \frac{a}{2}\right)\theta\left(|y-R_i^y| - \frac{a}{2}\right)\theta\left(|z-R_i^z| - \frac{a}{2}\right) \tag{B21}$$

with

$$\hat{J}_i^x = \frac{Ze}{m}\left[p_i + ZeA_x(R_i^x, R_i^y, R_i^z)\right] \tag{B22}$$

In all the calculations, we considered an high energy cutoff of 0.5 eV on the photon modes and checked convergence with the cutoff. In Fig. 5, we show an example of light-dressed linear response dynamics for the homogeneous position and momentum perturbations.

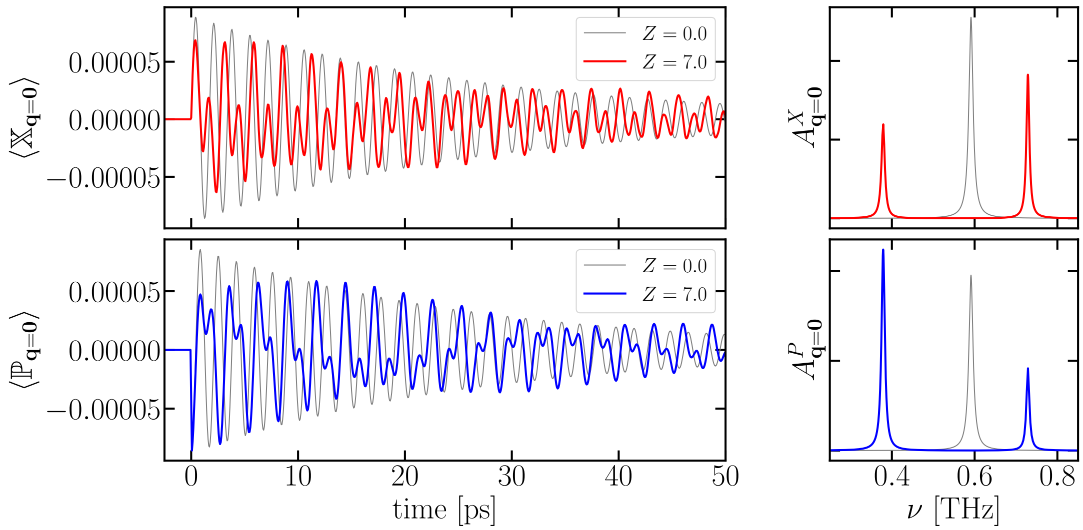

FIG. 5. Left panels: Linear response dynamics for the homogeneous $\mathbf{q} = \mathbf{0}$ position (top) and momentum (bottom) for increasing values of the effective charge. Right panels: Light-dressed position and momentum response function obtained by Fourier transform of the time signals.

a. Fluctuation in a toy model of two minimally coupled quantum oscillators

In order to understand the behaviour of the position and momentum fluctuations as a function of the light-matter coupling, we build a toy-model of two minimally coupled quantum oscillators. We introduce two sets of conjugate variables, (X_1, P_1) and (X_2, P_2), representing, respectively, the dipoles and the electromagnetic field. Here, X_2 plays the role of the vector potential operator, and P_2 the electric field operator. We therefore write a minimally coupled Hamiltonian akin to the full Hamiltonian in Eq. (B11)

$$H = \frac{1}{2}(P_1 + ZX_2)^2 + \frac{1}{2}X_1^2 + \frac{P_2^2}{2} + \frac{X_2^2}{2}. \tag{B23}$$

We diagonalize the Hamiltonian in Eq. (B23) and compute the position and momentum fluctuations of the dipole operators. In Fig. 6 we show that the toy model reproduces the enhancement/suppression of the momentum/position fluctuations discussed in the main text.

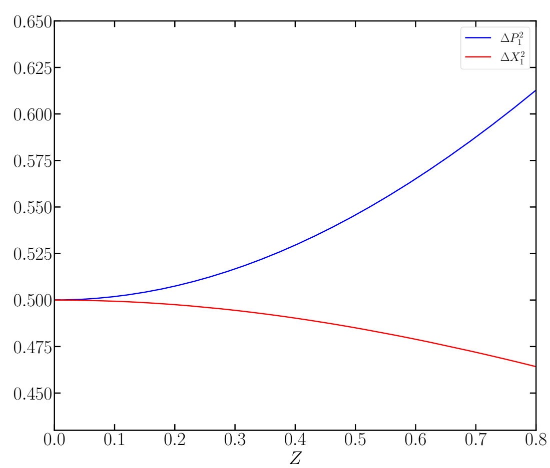

FIG. 6. Enhancement/suppression of the momentum/position fluctuations as a function of the coupling parameter, in the toy model in Eq. (B23).